

Inelastic-Tunneling Spectra of Organic Compounds*

Michael G. Simonsen and R. V. Coleman

Department of Physics, University of Virginia, Charlottesville, Virginia 22901

(Received 25 June 1973)

Inelastic electron tunneling has been studied in Al-Al₂O₃-Pb tunnel junctions doped with a wide range of organic compounds. These include simple straight-chain hydrocarbons, amino acids, aromatic ring compounds, pyrimidine bases, cyclic saturated hydrocarbons, and other nonaromatic ring compounds. The observed inelastic-tunneling spectra have been analyzed in terms of the expected vibrational modes of these molecules and results show that the method has sufficient sensitivity to differentiate many of the characteristic modes in these compounds. Comparison with Raman and infrared spectra have been made and a detailed analysis of this comparison is included. In general, the tunneling spectra often show a better over-all agreement with Raman spectra than with infrared spectra, but important differences exist between the different methods in a number of cases. In most cases the identification of specific modes in the tunneling spectrum is in quite good agreement with both the Raman and infrared spectra. The tunneling spectra have been recorded at 4.2 K in most cases, but improved resolution can be obtained near 1 K and preliminary examples are included. The doping has been accomplished using a combination of vacuum chambers which allows doping of successive junctions with different organic compounds without cross contamination. The experiments demonstrate that the inelastic-tunneling technique can be applied to a complete range of organic compounds and may prove to be highly useful technique for the analysis of very small quantities of material.

I. INTRODUCTION

A number of papers¹⁻⁴ have reported on the use of inelastic-electron tunneling as a tool for studying molecular excitations in organic molecules. These papers have reported results for a number of representative cases of simple acids and alcohols. Examples reported include methanol,² ethanol,² acetic acid,^{1,2} cyanoacetic acid,² propionic acid,^{1,2} and formic acid.³ Initial results on amino acids⁴ have been published by the present authors.

In this paper we report on a systematic study of a wider range of organic compounds including ring compounds as well as a number of straight-chain hydrocarbons. We have also compared the resulting tunneling spectrum to the corresponding infrared and Raman spectra measured for these same molecular species. The general comparison of the spectra has allowed us to evaluate the use of the tunneling method as an analytic tool as well as to compare similarities and differences between spectra obtained using tunneling, Raman, and infrared methods.

Previous work has usually been carried out by introducing the organic directly into the vacuum chamber in which the junction is fabricated. In order to ensure that contamination of the fabrication system by successive dopants does not occur we have used an apparatus in which the doping of the junction is carried out in a separate isolated vacuum chamber. This also allows a clean control junction to be fabricated following each run so that accidental contamination can be monitored.

The inelastic-electron-tunneling processes which

are responsible for the spectra observed in these experiments can in principle be connected with either infraredlike or Raman-like excitations since most of the molecules examined do not have a center of symmetry. Both mechanisms probably contribute an observable intensity in the tunneling experiments and some information on the relative strength of the two contributions may be deduced by evaluating the degree of agreement of the tunneling spectra with the infrared and Raman spectra.

To facilitate the comparison we have plotted both the infrared and Raman spectra along with the tunneling spectrum in cases where both are available. For presentation of the Raman spectra we have plotted vertical lines at the listed energies with heights proportional to the assigned intensities. Weak and very weak Raman modes have been omitted. This line-spectrum method of presentation has been used since some of the data are available only in the form of tables. Unless otherwise stated the infrared spectra have been taken from *The Aldrich Library of Infrared Spectra*,⁵ the Raman data from *TRC Selected Raman Spectral Data*⁶ and *The Raman Effect and its Chemical Applications*.⁷

We have used Al-Al₂O₃-Pb tunnel junctions for most of the work and the organic dopant has been added after the oxidation of the Al electrode and before the deposition of the Pb. The basic mechanism of inelastic tunneling will be briefly reviewed below followed by sections on the experimental methods and results of the present experiments. More complete reviews of electron-tunneling methods and experiments can be found in Ref. 8.

A. Inelastic-Tunneling Mechanism

The inelastic-tunneling process involves the tunneling of an electron from a state on the left of the barrier to a state on the right of the barrier with lower energy. At the same time the molecular impurity will be excited from its ground state to an excited state and the tunneling rate will be given by

$$W_{l \rightarrow r} = \frac{2\pi}{\hbar} |M_{rl}|^2 \delta(E_l - E_r - \hbar\omega_0), \quad (1)$$

where M_{rl} is the tunneling matrix element connecting the states on the right and left and $\hbar\omega_0$ is the energy of the molecular excitation. When the temperature is sufficiently low, the molecular impurities will all be in their ground state and the inelastic tunneling term will not involve electron backflow (anti-Stokes processes). As the voltage applied to the junction is raised from zero the onset of the inelastic-tunneling current therefore occurs when $eV = \hbar\omega_0$ and represents a one-way current to be added to the standard elastic-tunneling current.

The interaction of the electron with the molecular impurity can be a direct electron-molecular-dipole interaction in correspondence to an infrared absorption or it can be an electron-induced molecular-dipole interaction similar to a Raman-scattering process. The current contributed by the first process is proportional to the dipole moment or polarization \bar{P} associated with a particular molecular vibration while that of the second process is proportional to the induced dipole moment or polarizability α ($\bar{P} = \alpha\bar{E}$). Lambe and Jaklevic^{2,9} have considered both processes and the expressions for the contribution to the second derivative of the tunneling current with respect to the voltage, d^2I/dV^2 , are given by

$$(\text{ir}) \frac{d^2I}{dV^2} = NG_0A \sum_m |\langle m | P_x | 0 \rangle|^2 \delta(eV - \hbar\omega_m), \quad (2)$$

$$(\text{Raman}) \frac{d^2I}{dV^2} = NG_0B \sum_m |\langle m | \alpha | 0 \rangle|^2 \delta(eV - \hbar\omega_m), \quad (3)$$

where N is the total number of impurity molecules, G_0 is the constant conductance from elastic tunneling, and A and B are constants involving the barrier height and thickness. The quantities $\sum_m |\langle m | P_x | 0 \rangle|^2$ and $\sum_m |\langle m | \alpha | 0 \rangle|^2$ are summed over the spectrum of final states and should be compared to the absorption coefficient of light (ir) and intensity of scattered light (Raman). Lambe and Jaklevic^{2,9} have estimated these quantities to be of the same order of magnitude and of sufficient size to make both processes observable in a tunneling experiment.

Scalapino and Marcus¹⁰ have considered the electron-dipole interaction using a hydroxyl group near

a Pb-Al₂O₃ interface as an example. For a coverage of 10 hydroxyl groups per 100 Å² of surface they estimate the size of the conductance change to be on the order of 1%. They also point out that the dipole spectral weight function to be used in the intensity calculation is that appropriate to the molecule in its local environment including the influence of the metal-insulator surface. Therefore the observation of inelastic tunneling may offer a probe to study surface correlations of the metal as well as possible surface adsorption properties of the molecular impurity.

A number of factors can contribute to the resolution obtainable in inelastic-tunneling spectroscopy. One of these is temperature broadening and Jaklevic and Lambe⁹ have shown that for a single sharp molecular excitation, the second derivative of the inelastic tunneling current is given by

$$\frac{d^2I}{dV^2} = C \left(\frac{e^2}{kT} \right) e^v \left(\frac{(v-2)e^v + (v+2)}{(e^v-1)^3} \right), \quad v \equiv \frac{eV - \hbar\omega_0}{kT} \quad (4)$$

which is a symmetrical bell-shaped peak of width $5.4kT$. At 4 K, the natural width of most molecular lines is greater than $5.4kT$. However, other factors may contribute to the widths of the tunneling peaks making it advantageous to perform measurements at lower temperatures (approaching 1 K) in order to improve resolution.

For example, resolution can be improved by having one or both electrodes in the superconducting phase. Due to the very pronounced density-of-states peak at the edge of the superconducting energy gap, very sharp structure occurs in the second derivative which will affect the sharpness of the onset of the inelastic-tunneling current. A fivefold increase in resolution has been observed¹¹ for junctions with one or both metal electrodes superconducting as compared to the case in which both electrodes are in the normal state. In addition, if both electrodes are in the superconducting phase the kT broadening is substantially reduced at 1 K since 2Δ is on the order of $(10-20)kT$.

II. EXPERIMENTAL TECHNIQUES

All junctions were prepared in a specially constructed vacuum system equipped with oil diffusion pumps and liquid-nitrogen traps. The two pumping systems served separate vacuum chambers connected via a 2-in. gate valve. A roller-drawn carriage was mounted in the manifold connecting the two systems and could be operated by means of a rotary vacuum feedthrough. By means of this carriage substrates could be transferred between the separate chambers and positioned for either electrode deposition and barrier preparation or for doping with the molecular impurity. Aluminum and lead electrodes were deposited on 1×2 -cm

glass substrates through appropriate masks at pressures of $\sim 10^{-6}$ Torr. Tungsten filaments in contact with 99.999% Al wire or 99.999% Pb shot were used as sources. The aluminum electrode was deposited first to a thickness of 1.5–2 μm . The aluminum oxide barrier was then prepared by the glow-discharge method. In this procedure the substrate was exposed to the chamber environment but the aluminum film was shielded from direct exposure to the glow-discharge electrode. Typical conditions used for the glow-discharge were 50 mTorr of oxygen pressure and a voltage of 570 V maintained for 20 min.

After allowing 5–10 min for the films to cool following oxidation, the substrates were transferred without breaking vacuum to the center of the doping chamber which was surrounded by a liquid-nitrogen jacket. After remaining for about 45 min in the doping chamber at 10^{-6} Torr the substrate had cooled to approximately -40°C . A vapor of the dopant chemical was then introduced to the chamber for 10–15 min without pumping. Following doping, the chamber was pumped through liquid-nitrogen traps back to the initial pressure of approximately 10^{-6} Torr. The substrates were then returned through the gate valve to the metal-deposition chamber where the lead electrodes were evaporated.

For high-vapor-pressure compounds, the dopant was introduced into the doping chamber through a vacuum stopcock from a glass chamber equipped with heating tape. Exposure times were 10 min for most volatile chemicals.

For low-vapor-pressure chemicals the dopant was placed on a resistivity heated 0.001-in. Ta sheet located approximately 1.4 cm below the substrate. The temperature of evaporation was monitored with a thermocouple in contact with the Ta sheet. The temperature measurement was calibrated by observing the melting point of various dopants. The amount of dopant deposited on the junction is roughly indicated by the increase in junction resistance although no detailed calibration has been made. The undoped control junction prepared under the same conditions has a resistance in the range 10–100 Ω (measured at 4.2 K) while the doped junctions have resistances up to 50 000 Ω , for an area of 1 mm^2 , although we generally tried to adjust doping conditions to reach a final junction resistance between 5000–10 000 Ω . The various dopants and their sources are listed in Table I.

The tunnel-junction characteristics were measured by conventional harmonic techniques employing a bridge circuit similar to the one described in Ref. 12. The dc bias, with the Pb electrode positive, was swept from 0 to 500 mV using a slowly varying sine wave from a standard oscillator.

TABLE I. Chemical dopant and source.

Chemical	Source
Amino acids, Mann analyzed	Mann Research Labs
Pyrimidine bases, A grade	Calbiochem
Gallic acid, acetic acid, acetamide, Fisher certified	Fisher Scientific Co.
<i>p</i> -aminobenzoic acid, cyclohexanol, Aldrich analyzed	Aldrich Chemical Co., Inc.
Glycerol, Mallinckrodt analytical reagent	Mallinckrodt Chemical Works
Ethylene glycol, Baker analyzed reagent	J. T. Baker Chemical Co.
7, 7, 8, 8-tetracyanoquinodimethan	Eastman Kodak Co.

The bias was modulated with a 500-Hz ac voltage of 0.1–2.0 mV depending on the resistance of the junction. The 1000-Hz second-harmonic signal from the bridge was detected with a lock-in amplifier and the output was displayed on the Y axis of an X-Y recorder with the applied dc bias displayed on the X axis.

The specimens were immersed directly in liquid helium for the measurements at both 4.2 and 1.2 K. The entire apparatus was located in a shielded room isolated from the power-line ground and using filtered-power systems. The lock-in amplifier was operated in the selective external mode with a 1-sec time constant. Data were generally taken with the lock-in on the 20- μV sensitivity scale. The second-harmonic signal from the bridge is proportional to the second derivative of the junction current with respect to the applied dc voltage d^2I/dV^2 . Therefore the recorded curves show peaks whenever the bias voltage reaches values such that $eV = \hbar\omega_m$ and an onset of forward inelastic-tunneling current occurs due to excitation of the molecular vibration. With the Pb electrode in the superconducting state, the peak occurs at $eV = \hbar\omega_m + \Delta_{\text{Pb}}$ ($\Delta_{\text{Pb}} = 1.24$ meV). In the data presented below the bias voltage V is expressed as the numerically equivalent energy in units of electron volts. The corresponding wave-number scale is also indicated.

III. RESULTS AND DISCUSSION

A. General Features of Tunneling Spectra

An undoped junction (clean junction) shows prominent features which can be identified with electrode or barrier modes. A spectrum obtained from a control junction carried through the complete preparation process without doping is shown in Fig. 1.

The most prominent feature is the alumina hydrate OH bending mode at 920 cm^{-1} due to trace amounts of water vapor in the system that react with the aluminum oxide layer. Also present are the Al phonon peak at 320 cm^{-1} , the second harmonic of the hydrate OH bend at 1840 cm^{-1} , and the free-OH stretch at 3630 cm^{-1} . A CH-stretch mode

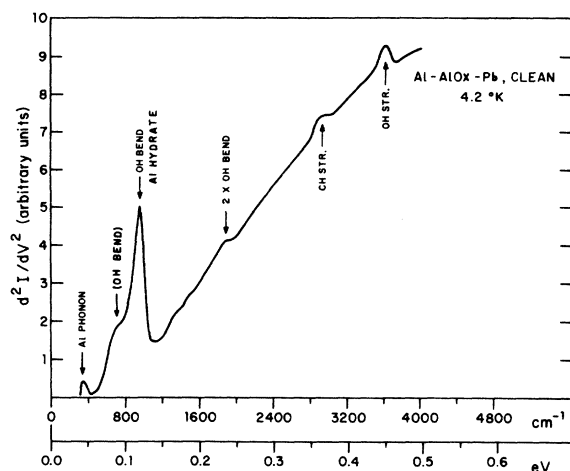


FIG. 1. Tunneling spectrum of a typical clean junction.

is also observed in a clean junction and probably arises from slight contamination of the junction by hydrocarbon pump oil.

The clean-junction control spectrum could certainly be improved by using more sophisticated preparation techniques, but we believe that the present level of residual structure does not materially affect the interpretation of the spectra ob-

tained from doped junctions.

All of the tunneling spectra obtained from junctions doped with organic molecules have certain major features which occur due to strong vibrational modes common to most hydrocarbons. For example, very strong CH-stretch modes are always observed in the range near 3000 cm^{-1} when this group is present in the molecule. Variations in the detailed structure and position of this mode are observed from molecule to molecule and these will be pointed out in specific cases. Other modes common to most doped junctions are the CH bend in the region of 1400 cm^{-1} and the CH-rocking modes in the range $400\text{--}800\text{ cm}^{-1}$.

When the molecule contains one or more OH groups we usually see a much enhanced free-OH stretch mode at 3630 cm^{-1} although as pointed out before this mode is usually weakly present in the undoped junction. Many spectra also exhibit evidence of an OH-bending mode near 1300 cm^{-1} .

Spectra characteristic of simple hydrocarbons are shown in Figs. 2-4. Figure 2 shows tunneling data taken at 4.2 K for ethylene glycol and glycerol which are two very similar molecules containing a minimum number of possible vibrational modes connected with CH, CH_2 , and OH groups. The chemical formula for each compound is indicated to the right of the tunneling curve. The CH-stretch

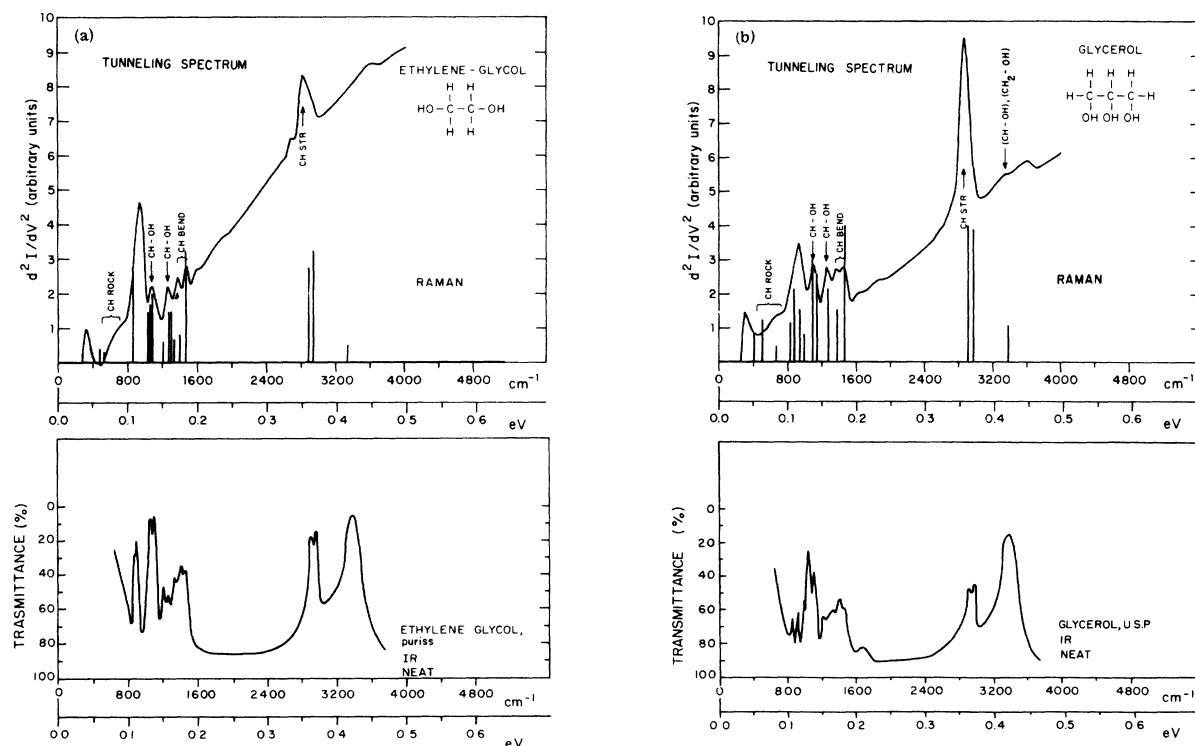


FIG. 2. Representative tunneling spectra of hydrocarbon doped junctions: (a) ethylene glycol, (b) glycerol. The Raman (Ref. 6) and infrared (Ref. 5) spectra are also included for comparison.

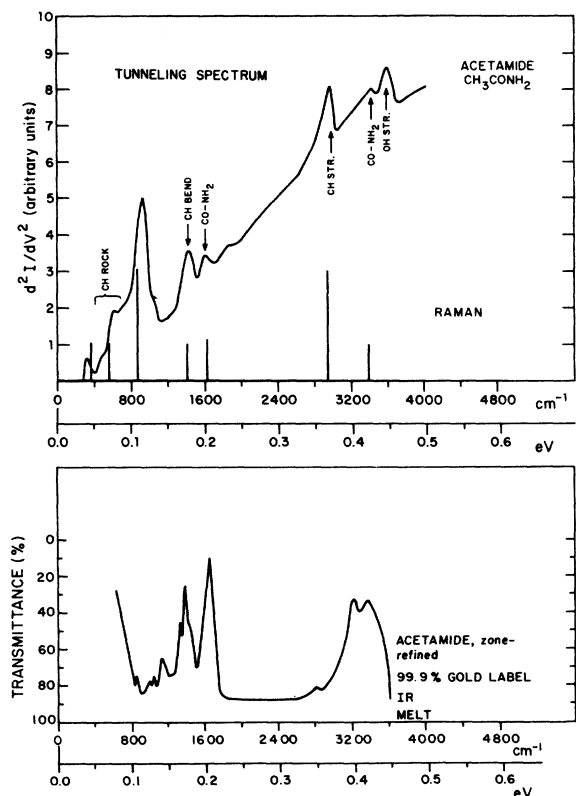


FIG. 3. Tunneling spectrum of acetamide. The Raman (Ref. 7) and infrared (Ref. 5) spectra are included for comparison.

mode at $\sim 2900 \text{ cm}^{-1}$ is the dominant feature at high energy while the OH-stretch mode is relatively weak. At lower energies CH bend and CH-OH-stretch modes appear to be well resolved as labeled in the figures. The observed tunneling peaks agree well with the positions and relative intensities of the Raman modes and these are indicated by the line spectrum plotted just below the tunneling curve. Infrared spectra are also included as shown in the lowest curve of each figure. The tunneling curves do not resolve as many modes as either the Raman or infrared spectrum, but the tunneling curve represents an accurate envelope of the observed Raman or infrared spectrum and the peaks of major intensity occur at similar energies. The resolution of the tunneling curve can be improved by reducing the temperature to $\sim 1 \text{ K}$ and some results will be discussed in a later section. Lower temperature can, for example, resolve the doublet structure of the CH-stretching peak which is not resolved in the tunneling spectrum of glycerol or ethylene glycol at 4.2 K . Strong CH bending modes are observed for glycerol between 1400 and 1600 cm^{-1} and their positions agree well with the Raman data. Deformation modes of the CH-OH moiety

are observed between 1000 and 1400 cm^{-1} and agreement with the Raman spectrum is quite good. Weak CH rocking vibrations appear to contribute below 800 cm^{-1} .

There is general agreement with the ir spectrum of glycerol below 1600 cm^{-1} except for the weak ir peak at 1200 cm^{-1} which is absent in the tunneling spectrum. A major discrepancy between the ir spectrum and both the tunneling and Raman spectra occurs in the OH-stretch region. A very strong ir OH-stretch mode is observed at 3350 cm^{-1} while the tunneling and Raman spectra have only weak modes in this region. This discrepancy is also evident in the case of ethylene glycol. It is possible that adsorption effects are in part responsible for this discrepancy. However, agreement of the intensity of the tunneling peaks with Raman intensities is a characteristic feature of many of the spectra as seen below.

The comments made on the glycerol spectrum concerning the 1000 – 1600-cm^{-1} region are also true for the ethylene glycol spectrum. The CH bend and CH-OH modes are observed to approximately agree with both ir and Raman data. Again, no tunneling mode occurs near 1200 cm^{-1} to match the ir mode at this energy; in this case a Raman

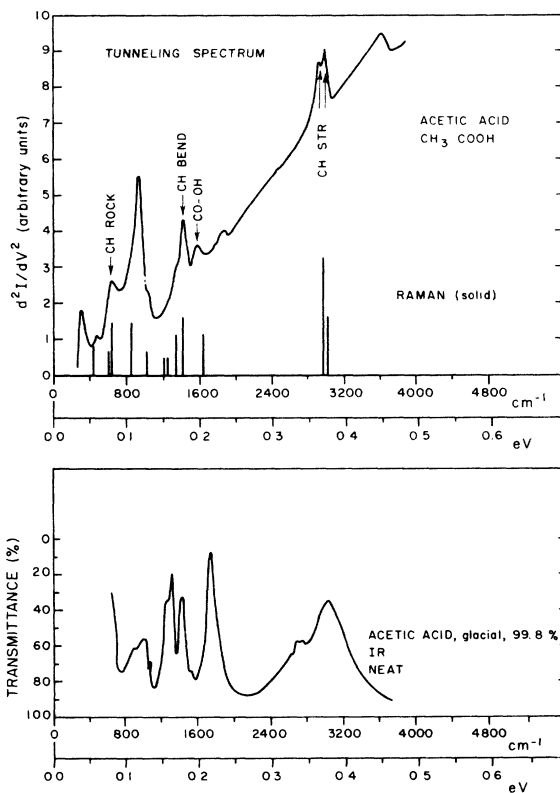


FIG. 4. Tunneling spectrum of acetic acid. The Raman (Ref. 7) and infrared (Ref. 5) spectra are included.

mode is also observed in this region. The only major difference between the tunneling spectra of glycerol and ethylene glycol occurs in the CH-stretch region. The CH-stretch mode of ethylene glycol is much weaker, and a weak additional mode occurs near 2850 cm^{-1} . However, the over-all similarity of the spectra of these two compounds is evident, as might be expected due to their similar molecular structure.

Characteristic modes of specific molecular groups appear in many of the spectra. An example is the NH_2 stretch mode at 3450 cm^{-1} in acetamide as shown in Fig. 3. The characteristic mode of the amide group is also present at 1600 cm^{-1} . It should be noticed that the agreement with the Raman spectrum is particularly good in this case due in part to the existence of widely spaced reasonably high intensity lines. The ir spectrum obtained from the melt is also closely similar, although a weak ir mode at 1120 cm^{-1} is absent in the tunneling spectrum. In addition, both the C=O double-bond peak in the $1600\text{--}1700\text{-cm}^{-1}$ range and the CH-stretch peak near 3000 cm^{-1} are shifted to higher energy in the ir spectrum as compared to the tunneling and Raman spectra.

Some difficulty is encountered in making assignments for peaks occurring in the 1600-cm^{-1} region. The spectra of most doped junctions show a mode in this region. Other authors have identified modes in this region as arising from carboxyl or ionized carboxyl groups. This identification is possible in a number of our spectra, but it does not hold in many cases such as acetamide and the pyrimidines. In these cases, other identifications are possible as noted in the figures. In particular, a peak in this region as previously mentioned is assigned to the amide mode in acetamide whereas in a number of other spectra the 1600-cm^{-1} absorption is identified with various double-bond modes. The occurrence of these modes due to different groups at approximately the same energy in conventional vibrational spectra complicates the assignments. In addition, second overtones of single-bond stretching modes often fall in this region. Infra-red spectra of these and similar organic compounds exhibit double-bond modes at approximately 1600 cm^{-1} while Raman spectra generally exhibit the double-bond modes at $\sim 1700\text{ cm}^{-1}$.

The tunneling spectrum of acetic acid is shown in Fig. 4 and is one of the organic compounds examined in earlier tunneling experiments.^{1,2} The tunneling spectrum agrees quite well with the Raman spectrum in position and relative intensity of the various modes whereas the agreement with the ir spectrum is somewhat poor. In particular, a tunneling mode (although weak) at 650 cm^{-1} coincides with the two moderately strong Raman modes in this region, while the ir shows no corresponding

absorption. Also the carboxyl modes of the tunneling and Raman spectra at $\sim 1600\text{ cm}^{-1}$ agree well in relative intensity, whereas the corresponding ir mode is much stronger and occurs at 1750 cm^{-1} . This discrepancy may, however, be due to the ionization states of the different specimens. A further discrepancy between the ir spectrum and the tunneling or Raman spectrum is the occurrence of a strong ir mode at 1300 cm^{-1} . The CH-stretching doublet is just resolved in this spectrum at 4.2 K .

B. Amino Acid Spectra

The tunneling spectra of the amino acids, while showing many of the general features observed in simpler compounds, exhibit unique additional structure which provides a ready identification of each acid from its spectrum. Tunneling spectra for the amino acids cysteine, serine, proline, and phenylalanine are shown in Figs. 5(a)–5(d). The Raman spectra have been taken from data in a paper by Garfinkel and Edsall.¹³ Modes are observed which arise from the various specific side groups of each compound. A good example is the strong C-S-stretch mode at $\sim 700\text{ cm}^{-1}$ in cysteine. The S-H-stretch mode is also observed at $\sim 2600\text{ cm}^{-1}$, but is fairly weak. Although these peaks are also present at these wave numbers in the Raman spectrum of cysteine, the intensities are much less in the tunneling spectrum than in the Raman spectrum.

Another mode characteristic of an amino-acid side group is the C-O stretch at 1100 cm^{-1} in serine. This peak is absent in the Raman but present as two peaks in the ir. The two peaks at 1300 and 1500 cm^{-1} in the serine spectrum may correspond to the two Raman peaks at 1240 and 1500 cm^{-1} which are the only significant Raman modes in this region and probably are due to OH and CH deformations, respectively. The ir spectrum shows five sharp peaks of moderate intensity in this region. The strong ir mode at 1600 cm^{-1} due to the amino-acid carboxyl group may correspond to the weak tunneling peak at this wave number while this mode occurs at 1700 cm^{-1} in the Raman spectrum. A weak tunneling mode possibly due to an N-H stretch occurs at $\sim 3500\text{ cm}^{-1}$ and has no observed Raman counterpart; the ir shows a mode nearby at 3450 cm^{-1} . It should be noted that the NH-stretch mode is generally weak in the Raman effect.

The spectrum of proline shows the characteristic CH-NH-CH mode at 1210 cm^{-1} . Comparison of this spectrum with the ir data shows that a major discrepancy occurs at 2400 cm^{-1} where a moderately strong ir peak occurs with no corresponding tunneling peak. The Raman spectrum also shows no mode in this region.

The spectrum of phenylalanine shows strong con-

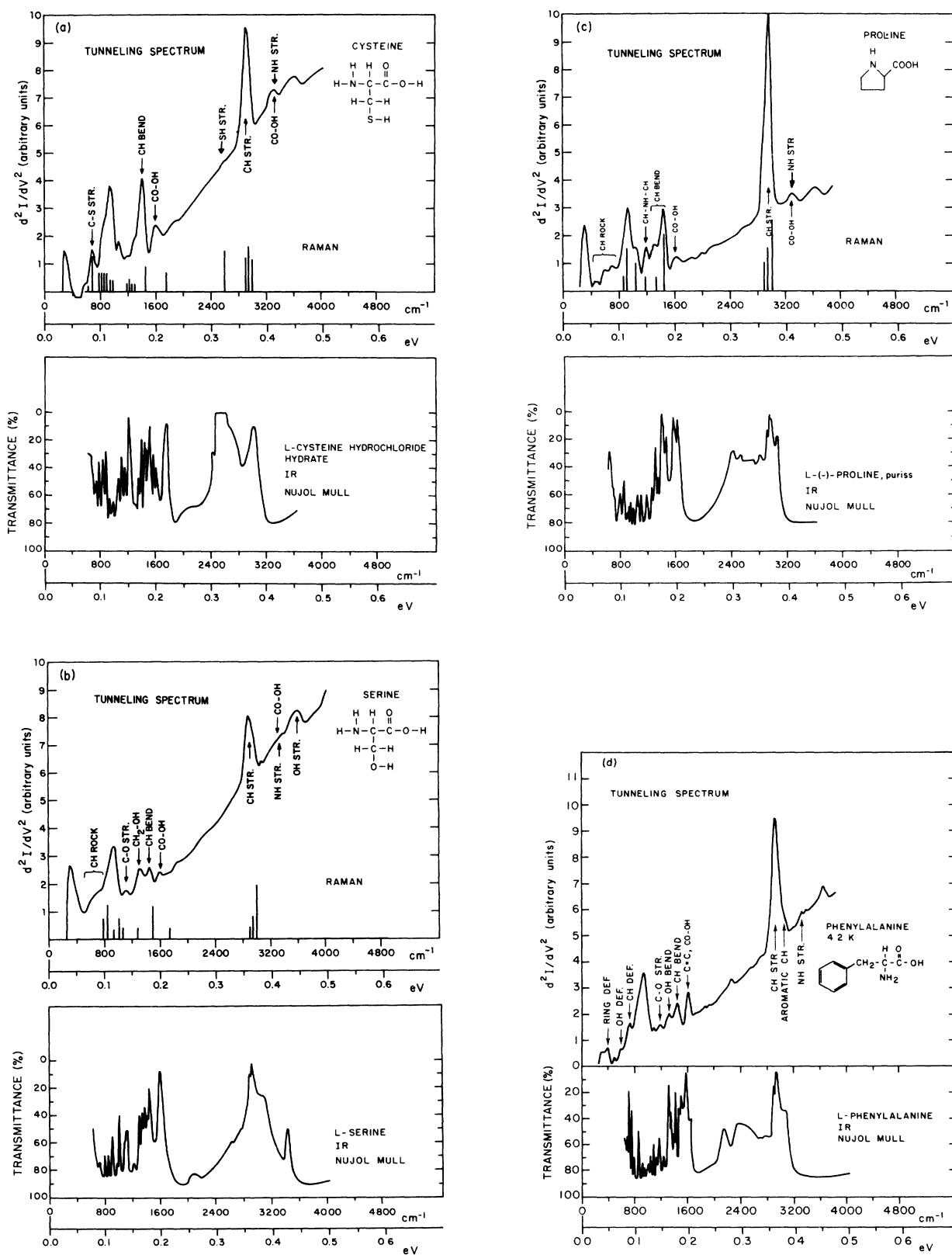


FIG. 5. Tunneling spectra of amino acids. The Raman (Ref. 13) and infrared (Ref. 5) spectra are included where available: (a) cysteine, (b) serine, (c) proline, (d) phenylalanine.

tributions from modes observed in the spectra of other hydrocarbon-doped junctions. Specifically, a strong CH-stretch peak occurs at 2900 cm^{-1} , the CH bend occurs at 1430 cm^{-1} , and the CH deformation mode is observed at 715 cm^{-1} . Also observed are the NH stretch at 3300 cm^{-1} , the OH bend at 1310 cm^{-1} , the C-O stretch at 1170 cm^{-1} , and the OH deformation at 590 cm^{-1} . Weakly observed in this spectrum are modes arising from the six-membered aromatic ring which constitutes the characteristic side group of phenylalanine. These modes, which occur with varying intensity in all the aromatic compounds studied, arise due to the interatomic vibrational coupling of the atoms constituting or bonded to the ring and will be discussed more fully in Sec. III C. The modes observed in the phenylalanine spectrum are the aromatic CH vibration at 3040 cm^{-1} and the ring deformation mode at 380 cm^{-1} . In addition, the ring double bonds contribute at 1600 cm^{-1} along with the C=O stretch of the amino-acid carboxyl group. The tunneling and ir spectra of this compound are in reasonably good agreement. However, discrepancies are observed in the $2000\text{--}2600\text{-cm}^{-1}$ range; the ir spectrum shows a peak at 2150 cm^{-1} and a broad absorption between 2300 and 2600 cm^{-1} while the tunneling spectrum has only a weak mode at 2230 cm^{-1} .

C. Spectra of Aromatic Ring Compounds

We have collected data on a number of simple ring compounds in an attempt to evaluate the sensitivity of the technique for identification of vibrational modes associated with the ring structure. Most of the data have been taken using compounds with a single six-member ring and comparisons have been made to the Raman and ir spectra obtained from the same molecules.

An example of the tunneling spectrum from the aromatic ring compound *p*-aminobenzoic acid is shown in Fig. 6 which also includes the ir spectrum for comparison. The general features of both the tunneling and ir spectra are in agreement and can be identified with specific vibrational modes. Distinctive structure is observed in the region of $2800\text{--}3100\text{ cm}^{-1}$ corresponding to modes associated with C-H-stretching vibrations. The aromatic ring compounds all show a doublet peak with a characteristic splitting of about 100 cm^{-1} in this region. This doublet peak probably arises due to CH vibrations involving stretching motions along the bond valence direction, possibly coupled with various combinations of CH deformation modes, ring bond stretching modes, and ring deformations. Such modes have been identified in the infrared and Raman spectra of benzene in the liquid and vapor states by Herzberg.¹⁴ These modes are quite complex even in the relatively simple case of benzene.

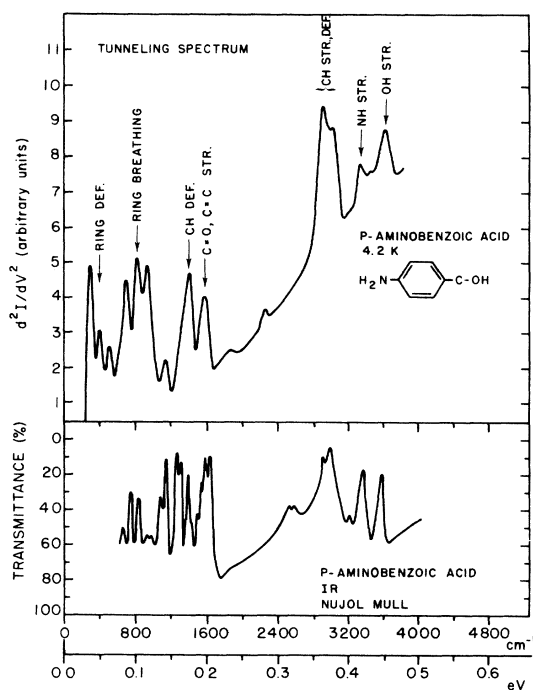


FIG. 6. Tunneling spectrum of *p*-aminobenzoic acid. The infrared spectrum (Ref. 5) is included below for comparison.

Therefore, a detailed analysis of the modes observed in the tunneling spectrum has not been attempted. Two higher energy peaks near 3300 and 3600 cm^{-1} associated with the N-H- and OH-stretching modes, respectively, are also observed.

In the lower energy range a distinct mode is observed at 1600 cm^{-1} and this can most probably be identified with strong double-bond stretching modes such as C=O and C=C as discussed previously. The ring C-H bending mode generally occurs near 1400 cm^{-1} and in the case of ring structures there are a number of skeletal ring modes which can also contribute intensity in this range. At energies near 1200 cm^{-1} a number of vibrations can contribute, complicating assignments in this region. Specifically, C-O and C-N stretching modes, modes arising from substitution of the aromatic ring, carboxyl group modes, and amine modes all occur in the region between 1100 and 1300 cm^{-1} . Therefore, the peak in the spectrum of *p*-amino benzoic acid at 1150 cm^{-1} may contain contributions from one or more of these modes, making its identification difficult. Measurements at lower temperatures may resolve these possible individual contributions. A strong ring breathing mode is generally identified as occurring near 800 cm^{-1} in Raman and ir spectra and this is also observed in the tunneling spectrum of Fig. 6.

Out-of-plane deformation modes can be observed

in the range 500–600 cm^{-1} and such peaks are observed in the tunneling spectra, but identification of the specific bonds involved is speculative at present.

Most ir spectra do not extend below $\sim 600 \text{ cm}^{-1}$ and Raman lines are generally very weak below 500 cm^{-1} . In all conjugated ring spectra so far measured by tunneling we see a strong mode near 400 cm^{-1} . This is probably a low-frequency ring mode involving a deformation of the ring, but has not been specifically identified. In the case of D_{6h} symmetry a mode occurs at 404 cm^{-1} identified with the $\nu_{20}^{C1}(e_{2u})$ mode of the ring.¹⁴ A similar mode will also occur in the less symmetric rings studied in the present experiments.

A further example of the tunneling spectrum of an aromatic ring compound is provided by the gallic acid spectrum shown in Fig. 7. Modes characteristic of the aromatic ring are observed here as in the *p*-aminobenzoic acid spectrum, but they are somewhat weaker and, in addition, small shifts in the positions of the peaks are observed. The two main peaks in the CH-stretch region are better resolved here, but the intensity of the higher-energy mode is considerably less. Also present with low intensity are the ring breathing mode at 780 cm^{-1} , and the tentative ring deformation mode at 390 cm^{-1} . The latter peak occurs at slightly lower energy than does the corresponding peak in *p*-aminobenzoic acid. A weak mode is observed at 1200 cm^{-1} whose identification is again difficult

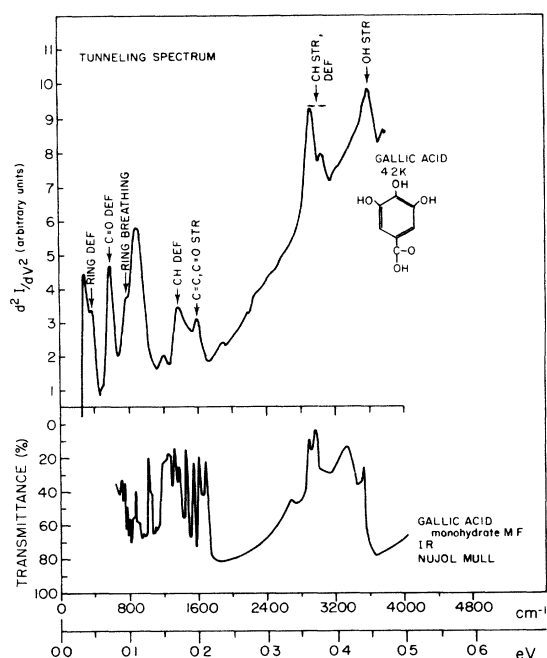


FIG. 7. Tunneling spectrum of gallic acid. The infrared (Ref. 5) spectrum is included.

and is further complicated by the fact that the phenolic OH group of gallic acid may contribute here.

Other readily identifiable modes in the gallic acid spectrum of Fig. 7 are contributions from the C=C and C=O stretch at 1580 cm^{-1} and the CH deformation at 1370 cm^{-1} . Skeletal ring modes may as previously mentioned also contribute to the bands in the CH deformation region. Characteristic modes of the gallic acid molecule occur at 3600 cm^{-1} and at 600 cm^{-1} . The strong mode at 3600 cm^{-1} results from the stretching vibrations of the three OH substituent groups while the 600- cm^{-1} mode may be tentatively assigned to a C=O out-of-plane deformation mode.¹⁵

D. Nonaromatic Ring Compounds

As an example of a cyclic saturated hydrocarbon (cycloalkane) the tunneling spectrum of the six-membered ring compound cyclohexanol is shown in Fig. 8. The tunneling spectrum is in excellent agreement with the Raman and ir spectra which are also shown in Fig. 8. The high-energy modes are in one-to-one correspondence while all three spectra show a large number of modes below 1600 cm^{-1} . The tunneling spectrum does not resolve all of the modes below 1600 cm^{-1} , but certainly indicates the presence of the major modes giving correct energies and relative intensities. The CH-stretching mode is split into two peaks corresponding to the symmetric and asymmetric stretching modes of the CH_2 groups. The peak at $\sim 2850 \text{ cm}^{-1}$ corresponds to the symmetric mode and the peak near 2900 cm^{-1} corresponds to the asymmetric mode. This split peak can be more completely resolved in the tunneling spectrum by reducing the temperatures to approximately 1 K as shown in the insert of Fig. 8. The Raman and ir spectra both agree well with the position and intensity of the CH-stretch modes as identified in the tunneling spectrum. A weak mode is also observed at $\sim 2550 \text{ cm}^{-1}$. This mode is resolved at the same energy in the Raman and ir spectra and probably corresponds to a secondary band similar to those identified in the 2600–2800- cm^{-1} range for the symmetric cycloalkane, cyclohexane (C_6H_{12}).¹⁶ The major discrepancy observed in the high-energy region is the fact that while the ir spectrum shows a very strong OH stretch near 3400 cm^{-1} , the tunneling spectrum has only a very weak mode in the region; the Raman spectra has no mode with assigned intensity at this position.

At lower energies the tunneling spectrum shows a fairly intense mode at 1450 cm^{-1} in agreement with both the Raman and ir spectra. This corresponds to the scissoring mode of the CH_2 group and is the most characteristic C-H deformation mode observed in cyclic saturated hydrocarbons.

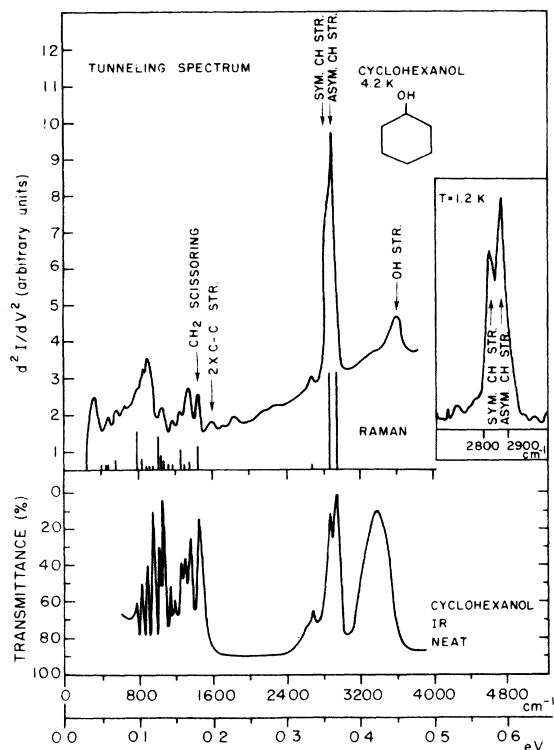


FIG. 8. Tunneling spectrum of cyclohexanol. The insert shows data from the same junction taken at 1.2 K in the CH-stretch region on an expanded energy scale. The Raman (Ref. 6) and infrared (Ref. 5) spectra are also included.

A mode probably identifiable as a C-O stretch occurs with moderate intensity at 1060 cm^{-1} due to the phenolic OH substituent group, while the weak mode at 1260 cm^{-1} may arise from the OH bending vibration of this group. A C-C stretch mode occurs at 800 cm^{-1} which is analogous to the ring breathing mode observed in aromatic compounds. The second overtone of this mode is observed at 1600 cm^{-1} in the tunneling spectrum. The other modes observed in the cyclohexanol spectrum are not readily identifiable due to a lack of tunneling data for other unconjugated ring compounds.

In addition, a number of other deformation modes are possible in the range $900\text{--}1350\text{ cm}^{-1}$. These have been calculated and specifically identified in the spectrum of cyclohexane¹⁶ which has the chair conformation (D_{3h} symmetry) as the dominant configuration. The spectrum of cyclohexanol has a number of additional lines, which can generally be analyzed in terms of the same type of modes. Ring modes have also been identified in a number of cycloalkanes and in the tunneling spectrum of cyclohexanol the peaks observed below 600 cm^{-1} indicate the possible presence of ring modes. Further discussion on the vibrational spectra of

cycloalkanes can be found in Ref. 16.

As a second example of a compound possessing a nonaromatic ring, the spectrum of 7, 7, 8, 8-tetracyanoquinodimethan (TCNQ) is presented in Fig. 9. In this spectrum the doublet structure similar to that observed in aromatic compounds and pyrimidine bases occurs in the $2800\text{--}3100\text{ cm}^{-1}$ range. The ring breathing mode is weakly evident at 850 cm^{-1} , and a strong mode occurs near 550 cm^{-1} which may arise due to ring deformations although various group deformations are also possible identifications. The mode at 720 cm^{-1} is probably assignable to a CH deformation vibration.

The moderately strong mode at 1330 cm^{-1} is most likely due to the ring CH bending vibrations although it occurs at anomalously low energy. The ring C=C bonds contribute near 1600 cm^{-1} , while the weaker peak at 1525 cm^{-1} is tentatively identified with the ring substituent C=C bonds.

A very prominent peak occurs at 2160 cm^{-1} due to the stretching of the four C≡N groups of TCNQ. The characteristic peak of the C≡N triple bond has also been observed in the tunneling spectrum of cyanoacetic acid,² and is generally narrow and of high intensity. Also observed in the TCNQ spectrum is an intense OH-stretch mode at 3630 cm^{-1} , indicative of excess water in the dopant.

In order to further test the tunneling technique as applied to ring compounds, we have obtained data on pyrimidine bases and spectra for the three bases uracil, cytosine, and thymine are presented below.

E. Pyrimidine Spectra

The tunneling spectra of the pyrimidines generally show the same modes as discussed for *p*-aminobenzoic acid and gallic acid. With some exceptions,

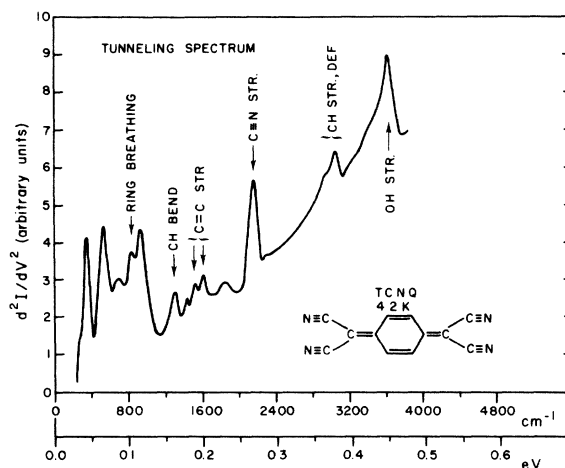


FIG. 9. Tunneling spectrum of 7,7,8,8-tetracyanoquinodimethan (TCNQ).

the observed pyrimidine modes are in agreement with ir and Raman spectral data although the comparison with the ir spectra is hampered by the fact that the ir spectra are taken using a Nujol-Mull technique.¹⁷ The tunneling spectra for cytosine, uracil, and thymine are shown in Figs. 10(a)-10(c). The Raman lines listed by Lord and Thomas¹⁸ are indicated by the line spectrum. These were mea-

sured in solution and do not extend much above 1600 cm^{-1} due to solvent effects. The ir spectrum of each compound is also plotted in Fig. 10.

The tunneling modes common to the pyrimidines and to the aromatic compounds studied are well resolved in the spectrum of cytosine shown in Fig. 10(a). The 420- cm^{-1} peak, tentatively assigned to a ring deformation, is quite pronounced. A weak mode occurs at 600 cm^{-1} which may arise due to out-of-plane deformations in analogy to the modes observed in this region for gallic acid and *p*-amino-benzoic acid. In the case of the pyrimidines, this mode may be specifically identified as a C=O deformation corresponding to the two Raman modes at 560 and 595 cm^{-1} in cytosine which have been tentatively identified as such by Lord and Thomas.¹⁸ The peak at 790 cm^{-1} may correspond to a ring breathing mode as in the aromatics and in agreement with the Raman identification for the strong peak at this wave number by Lord and Thomas.¹⁸ However, in the ir spectrum of uracil the modes in this region are attributed by Angell¹⁹ to C-H deformations, with the ring breathing mode being weak or unobservable and this may also apply to cytosine. This must therefore be considered as a possible alternative identification, especially since the intensity of the tunneling mode is in better

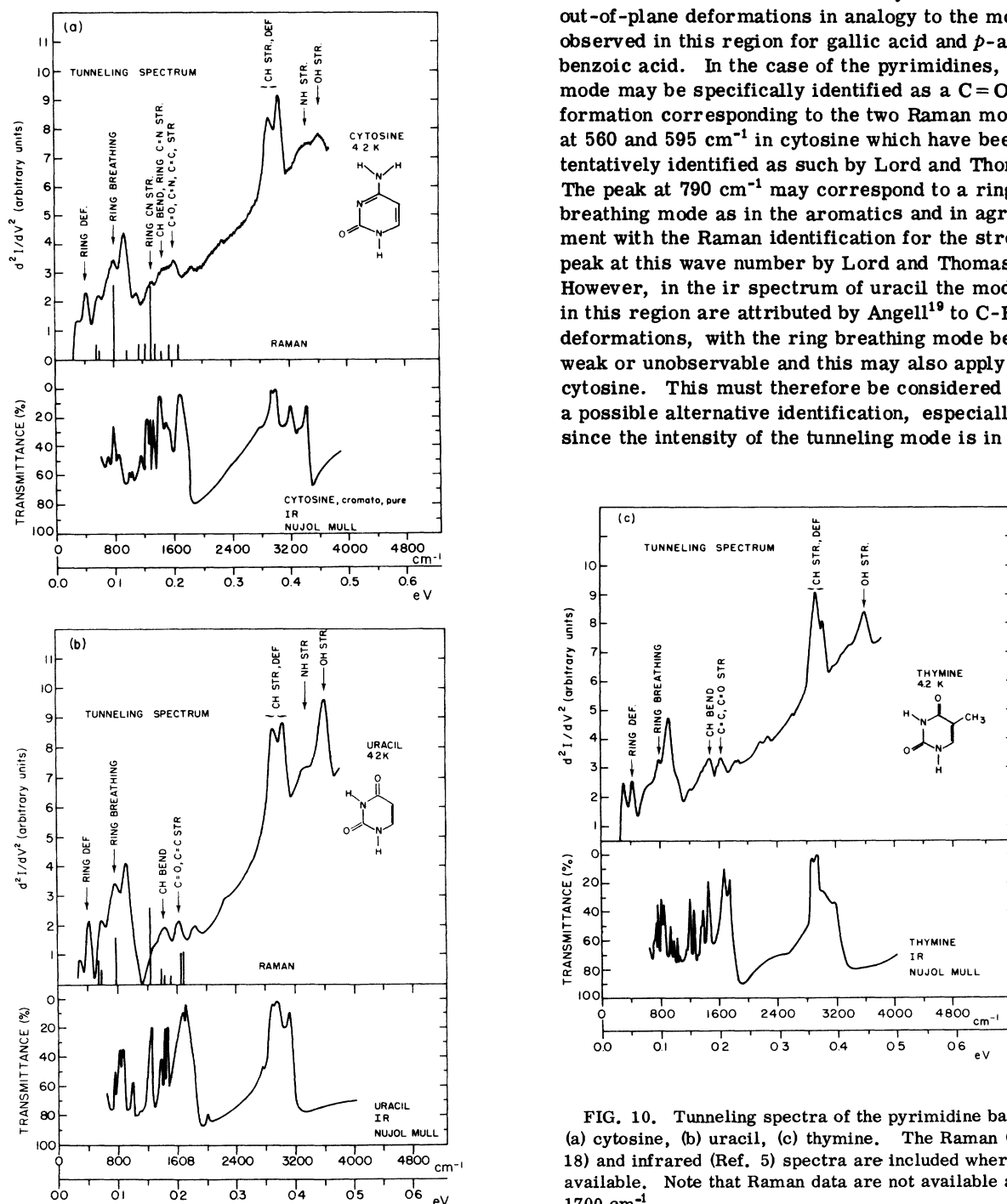


FIG. 10. Tunneling spectra of the pyrimidine bases: (a) cytosine, (b) uracil, (c) thymine. The Raman (Ref. 18) and infrared (Ref. 5) spectra are included where available. Note that Raman data are not available above 1700 cm^{-1} .

agreement with the ir than with the Raman intensity in this case.

The peak at 1300 cm^{-1} may correspond to the stretching modes of the cytosine ring observed in the Raman spectrum near this energy. However, the intensities do not agree well and some Raman peaks observed in this region do not appear in the tunneling spectrum. Infrared peaks also occur in this region, but again the agreement with the tunneling spectrum is not exact. As discussed below, discrepancies with the ir and Raman data also occur for the other pyrimidine spectra in this region. Therefore, any specific assignments of the tunneling modes are not certain on the basis of present data.

A broad absorption occurs between 1400 and 1550 cm^{-1} which encompasses a number of ir and Raman modes in this region. Modes in this region are identified¹⁸ with skeletal ring $\text{C}=\text{N}$ stretching in the Raman and ir analysis of cytosine derivatives, and therefore these may be the modes responsible for the tunneling peak observed here along with some contribution from the CH bend. A moderately strong peak occurs at 1630 cm^{-1} which may contain contributions from a number of double-bond modes including $\text{C}=\text{O}$, $\text{C}=\text{N}$, and $\text{C}=\text{C}$ stretching vibrations, plus coupled vibrations of these modes with each other and with the NH_2 scissoring mode.¹⁸ However, the individual contributions are not separately resolvable.

Two very distinct peaks occur in the $2900\text{--}3100\text{ cm}^{-1}$ region at positions previously observed in the aromatics. The higher-energy mode of this pair is much stronger and better resolved in cytosine than in the other aromatics. Although the relative intensities of these two peaks have been observed to vary from specimen to specimen, it is probable that the intensities can be correlated with the specific electronic distribution in the different pyrimidine rings.

A broad absorption occurs in the $3200\text{--}3400\text{ cm}^{-1}$ range which can be assigned to NH -stretching vibrations, with contributions from both the NH_2 and the ring NH groups.

The tunneling spectrum of uracil exhibits many of the modes observed for cytosine. The region below 800 cm^{-1} is quite similar for both compounds and the Raman and tunneling spectra of uracil in this region are in good agreement. Both show a single mode of medium intensity at 770 cm^{-1} , whereas the Nujol-Mull ir spectrum has two peaks of medium intensity at 825 and 865 cm^{-1} in addition to the weaker 770 cm^{-1} mode. The tunneling spectrum of uracil exhibits two well-resolved peaks in the CH stretch region as observed for cytosine, as well as the weak NH stretch centered near 3300 cm^{-1} .

Major differences between the uracil and cyto-

sine spectra occur between 1000 and 1600 cm^{-1} . Uracil exhibits only two peaks in this region, both of which are of medium intensity. The 1400 cm^{-1} mode is probably due to CH deformations, and the 1620 cm^{-1} mode is identified with $\text{C}=\text{C}$ and $\text{C}=\text{O}$ stretching vibrations. In contrast to the cytosine spectrum, very little absorption occurs in the interval between these modes due to the absence of the $\text{C}=\text{N}$ double bond in the ring, and the two modes observed in cytosine at 1100 and 1300 cm^{-1} are absent here. It is interesting that a peak is not observed near 1200 cm^{-1} for uracil, since both the ir and Raman spectra exhibit very intense peaks in this region due to ring CN -stretching vibrations.

The tunneling spectrum of thymine is quite similar to that of uracil except in the CH-stretch region where the methyl group contributes strongly at 2900 cm^{-1} , somewhat obscuring the 3040 cm^{-1} peak.

IV. CONCLUSIONS

These experiments demonstrate that the inelastic tunneling technique can be applied to a wide variety of chemical compounds. Stability to heating during the doping process has not so far appeared to cause difficulty, as the spectra show no evidence of breakdown of the dopants. Such breakdown is not expected since the temperatures required for sufficient doping have been from 50 to 100°C below the melting or decomposition temperatures. The spectra exhibit easily discernible differences between various compounds and demonstrate the potential of the method as an analytical tool for very small quantities of material (less than a monolayer on an area of $0.1\text{--}1.0\text{ mm}^2$).

The comparison with Raman and ir spectra indicates that the tunneling spectra are in better over-all agreement with Raman spectra, although many specific modes are found to be in good agreement with both infrared and Raman. However, important differences are observed in a number of cases. Due to the low symmetry of the molecular species studied, most modes are both ir- and Raman-active, and a definitive determination of the type or existence of selection rules obeyed by the tunneling mechanism is at present not possible. Theoretically, both the ir and Raman effects should contribute about equally to the tunneling spectra and further experiments should provide a better understanding of the inelastic-tunneling interaction. The generally good agreement of the observed intensities in the Raman spectra with those of the tunneling spectra are indicative that the Raman-like interaction may be important in the tunneling mechanism.

It should be noted that, although the tunneling spectra show good agreement with both ir and Raman spectra, there are nevertheless many cases

in which a tunneling peak is shifted relative to its supposed ir or Raman counterpart by an amount well above experimental error. While the full explanation of such shifts may require a better understanding of the inelastic-tunneling mechanism, it is possible that they are due in part to intermolecular interactions with neighboring dopant molecules, or with the alumina barrier or metal electrodes. In this regard, the frequently observed shift of the tunneling mode of the carboxyl group to lower wave number than the corresponding ir or Raman modes may be indicative of molecular aggregation. Such an effect has been observed in Raman studies of liquid samples (i. e., a downshift of the carboxyl mode with increased concentration of specimen), and has been attributed to intermolecular hydrogen bonding.⁷ In the tunneling experiments, hydrogen bonding with both neighboring dopant molecules (in heavily doped junctions) and with the alumina barrier or metal electrodes is a possibility.

It has often been suggested that surface adsorption mechanisms could be studied by observation of perturbations of molecular spectra in doped tunnel junctions. Such effects may play a role in

producing the shifts which we observe by altering molecular conformations and bond strengths in the dopant molecules. However, no definite evidence of this has been observed in the present experiments since many of the group frequencies, whether shifted or not, occur at approximately the same energy in a wide variety of molecular species. If adsorption of the dopant causes significant perturbations it would be surprising that such a wide variety of compounds produce similar adsorption shifts for the same modes. It is more likely that adsorption shifts are quite variable and specific to individual modes in specific compounds while in general major high-intensity modes remain relatively unshifted.

ACKNOWLEDGMENTS

The authors would like to thank Professor J. E. Coleman and Professor R. C. Morris for many helpful discussions. Werner Frewer and W. Walton have made valuable contributions to the construction of the apparatus and W. L. Sands designed and fabricated the special glass-bellows liquid-nitrogen trap used in the apparatus.

*Work supported in part by the U. S. Atomic Energy Commission under Contract AT-(40-1)-3105 and in part by the National Science Foundation under Contract No. GB 13344.

¹R. C. Jaklevic and J. Lambe, Phys. Rev. Lett. **17**, 1139 (1966).

²J. Lambe and R. C. Jaklevic, Phys. Rev. **165**, 821 (1968).

³J. Klein, A. Leger, M. Belin, D. DeFourneau, and M. J. L. Sangster, Phys. Rev. B **7**, 2336 (1973).

⁴Michael G. Simonsen and R. V. Coleman, Nature **244**, 218 (1973).

⁵Charles J. Pouchert, *The Aldrich Library of Infrared Spectra* (Aldrich Chemical Co., Cedar Knolls, N. J., 1970).

⁶*TRC Selected Raman Spectral Data* (Texas A and M University, College Station, Texas, 1965), Serial Nos. 1-54.

⁷James H. Hibben, *The Raman Effect and Its Chemical Applications* (Reinhold, New York, 1939).

⁸*Tunneling Phenomena in Solids*, edited by E. Burstein and S. Lundquist (Plenum, New York, 1969).

⁹R. C. Jaklevic and J. Lambe, in Ref. 8, p. 243.

¹⁰D. J. Scalapino and S. M. Marcus, Phys. Rev. Lett. **18**, 459 (1967).

¹¹I. Giaever, H. R. Hart, Jr., and K. Megerle, Phys. Rev. **126**, 941

(1962).

¹²J. G. Adler, T. T. Chen, and J. Straus, Rev. Sci. Instrum. **42**, 362 (1971).

¹³David Garfinkel and John T. Edsall, J. Am. Chem. Soc. **80**, 3823 (1958).

¹⁴Gerhard Herzberg, *Infrared and Raman Spectra of Polyatomic Molecules* (Van Nostrand, Princeton, N.J. 1968).

¹⁵L. J. Bellamy, *The Infrared Spectra of Complex Molecules*, 2nd ed. (Wiley, New York, 1958).

¹⁶Margareta Avram and GH. D. Mateescu, *Infrared Spectroscopy* (Wiley, New York, 1972).

¹⁷A dried powdered sample of the compound is mixed with liquid paraffins (Nujol) to produce a liquid-mull sample which is transferred to a window of NaCl. The spectrum of Nujol is superimposed upon that of the sample and this method cannot be readily used to analyze spectral regions where CH modes contribute.

¹⁸R. C. Lord and G. J. Thomas, Jr., Spectrochim. Acta A **23**, 2551 (1967).

¹⁹C. L. Angell, J. Chem. Soc. 504 (1961).